

DNA Self-Assembly and Computation Studied with a Coarse-grained Dynamic Bonded Model

Carsten Svaneborg¹, Harold Fellermann^{1,2}, and Steen Rasmussen^{1,3}

¹ Center for Fundamental Living Technology, Department of Physics, Chemistry and Pharmacy, University of Southern Denmark, Campusvej 55, DK-5320 Odense, Denmark, science@zqex.dk

² Complex Systems Lab, Barcelona Biomedical Research Park, Universitat Pompeu Fabra, Dr. Aiguadé 88, 08003 Barcelona, Spain, harold@sdu.dk

³ Santa Fe Institute, 1399 Hyde Park Road, Santa Fe NM 87501, USA, steen@sdu.dk

Abstract We study DNA self-assembly and DNA computation using a coarse-grained DNA model within the directional dynamic bonding framework [C. Svaneborg, *Comp. Phys. Comm.* 183, 1793 (2012)]. In our model, a single nucleotide or domain is represented by a single interaction site. Complementary sites can reversibly hybridize and dehybridize during a simulation. This bond dynamics induces a dynamics of the angular and dihedral bonds, that model the collective effects of chemical structure on the hybridization dynamics. We use the DNA model to perform simulations of the self-assembly kinetics of DNA tetrahedra, an icosahedron, as well as strand displacement operations used in DNA computation.

1 Introduction

Sequence specific hybridization of DNA single strands makes DNA molecules a flexible programmable building block. By choosing the right sequences, DNA self-assembly behavior can be programmed to produce well defined nano-structures. In the pioneering work of Seeman et al., branched DNA constructs have been utilized to self-assemble into a variety of structures [32,8,36,35]. With DNA origamis Rothemund invented a way to fold long DNA single strands into well defined planar structures by adding a large number of short stabilizing oligomer strands[26]. Later it was demonstrated how to let the planar origamis self-assemble into 3D nano-structures such as a box [2]. Ever since the pioneering work of Adleman in 1994 [1], DNA has also been recognized as a massively parallel, versatile, and inexpensive computing substrate. In order for such substrate to be of practical interest, however, it is desirable that the computational framework is scalable and that individual computational elements can be combined to form circuits. Recently, a scalable approach to enzyme-free DNA computing has been proposed where circuits consist of relatively short DNA strands that communicate via strand displacement [31,25].

The Poland-Scheraga (PS) model has been very successful in predicting thermal melting and renaturing of long DNA strands [24,13]. It describes a DNA

double strand as a 1D lattice where each base-pair is either hybridized or open. To each state is associated a free energy that has a sequence specific contribution from nearest neighbor interactions [29] as well as a polymer contribution from the conformational entropy of internal bubbles and frayed ends. Generalizations of the PS model exists, where the single strands are represented as semi-flexible polymers on a 3D lattice [12,14]. This provides a conceptual simplification since the polymer free energy contributions are given implicitly. The Dauxois-Peyrard-Bishop[22] (DPB) model represents a DNA double strand as a 1D lattice, but each base-pair is described by a continuous base-pair extension. The DPB model is defined by a Hamiltonian which includes a hybridization potential and a harmonic term penalizing deviations between nearest neighbor extensions.

The chemical structure of short DNA oligomers can be studied with atomistic molecular dynamics simulations such as Amber[6,7] and Charmm[4,17]. However, if we are interested in mesoscopic properties of long DNA molecules, it is more effective to utilize coarse-grained simulation models. Coarse-graining is the statistical mechanical process by which microscopic details are systematically removed, producing an effective mesoscopic model [16,21]. The major computational advantage of coarse-graining is that it allows us to focus our computational resources on studying the structures and dynamics at the mesoscopic level.

Coarse-grained models describe a nucleotide by a small number of effective interaction sites. In the “three site per nucleotide” model of de Pablo and co-workers, three sites represent the phosphate backbone site, the sugar group, and the base, respectively[28,27]. There is also a number of “two site per nucleotide” models, e.g. the model of Ouldrige and co-workers [19,20], where one site represents the base and another site the backbone and the sugar ring. Savelyev and Papoian [30] have formulated a “one site per nucleotide” model. As the number of interaction sites per nucleotide is reduced, the chemical structure is progressively lost. In simulations of DNA tagged nanoparticles, even more coarse-grained models are used. DNA molecules have been modeled e.g. as semi-flexible polymers with attractive sites on each monomer [11], or as a single sticky site that can be hybridized with free complementary free sticky sites [18]. While the chemical structure of DNA has been completely eliminated, these models still retain the DNA sequence specific hybridization effects on nanoparticle self-assembly.

We are interested in studying the statistical mechanics of hybridizing DNA strands and in particular the kinetics of DNA self-assembly and DNA computation using a DNA model that is as coarse-grained as possible. We have implemented a general framework allowing directional bonds to be reversibly formed and broken during molecular dynamics simulations[33]. Along with the bonds, the angular and dihedral interactions required to model the residual effects of chemical structure are also dynamically introduced and removed as dictated by the bond dynamics. This framework allows us to simulate reversible hybridization of complementary beads and chains built from such beads. In the present paper, we study a minimal dynamic bonding DNA model. For simplicity, we assume that the binding energy, as well as the bond, angular, and dihedral po-

entials are independent of sequence, and we have chosen a force field that produces a flat ladder-like structure in the double stranded state. Our motivation for these choices are to minimize the number of parameters required to specify the DNA model.

Dynamic bonding DNA models combine ideas from most of the existing DNA models. We regard them as dynamic generalizations of statistical mechanical theories and simultaneously as simplifications of coarse-grained DNA models. As in the PS model, a complementary base-pair can either be hybridized or open. When a base-pair is hybridized, it is characterized by a continuous hybridization potential as in the DPB model. Dynamic bonding DNA models can also be regarded as off-lattice generalizations of the lattice PS model [12]. Rather than trying to model chemical structure with interaction sites as in the “two and three site per nucleotide” models [28,27,19,20] dynamic bonding DNA models use angular and dihedral interactions to model the residual effects of local chemical structure. Dynamic bonded DNA double stands can reversibly melt and reanneal, which is not possible with the “one site per nucleotide model” of Savelyev and Papoian [30]. Finally, as in the sticky DNA models[18], a single bead in a dynamic bonding DNA model can equally well represent a domain.

Sect. 2 presents the dynamic bonding DNA model, which is used in Sect. 3 to study self-assembly of DNA constructs and DNA-computing constructs. Sect. 4 ends the article with a conclusions.

2 Dynamic bonding DNA model

In the present dynamic bonding DNA model, single stranded DNA (ssDNA) is represented by a string of nucleotide beads connected by stiff springs representing directional backbone bonds. Instead of using a four letter alphabet representing the ACGT nucleotides, in the present paper we increase the alphabet maximally to avoid getting trapped in transiently hybridized states. Physically, this corresponds to assuming that each bead represents a short sequence of nucleotides i.e. a domain, and that two non-complementary beads or domains are unable to hybridize. A novel feature of our DNA model is that it involves dynamic hybridization bonds, which are introduced or removed between complementary interaction sites or beads when they enter or exit the hybridization reaction radius. Along with the bonds, we dynamically introduce or remove angular and dihedral interactions in the chemical neighborhood of a hybridizing bead pair. These interactions are introduced based on the local bond and bead type pattern, and hence allows us to retain some effects of the local chemical structure in coarse-grained models. We utilize bonds carrying directionality to represent the 3'-5' backbone structure of DNA molecules. This allows us to introduce dihedral interactions that can distinguish between parallel and anti-parallel strand alignments. We have implemented this framework in a modified version of the Large-scale Atomic/Molecular Massively Parallel Simulator (LAMMPS) [23,33].

The DNA model relies on two ingredients, a Langevin dynamic for propagating a system in time and space, and a dynamic directional bonding scheme [33]

that propagates the chemical structure of the system. The force on bead i is given by a Langevin equation

$$\mathbf{F}_i = -\nabla_{\mathbf{R}_i} U - \frac{m}{\Gamma} \dot{\mathbf{R}}_i + \xi_i \quad \text{with} \quad U = U_{\text{bond}} + U_{\text{angle}} + U_{\text{dihedral}} + U_{\text{pair}}.$$

Here, the first term denotes a conservative force derived from the potential U . The second term is a velocity dependent friction, and the third a stochastic driving force characterized by $\langle \xi_i(t) \xi_j(t') \rangle = k_B T m / (\Gamma \Delta t) \delta_{ij} \delta(t - t')$. The potential U comprises four terms representing bond, angular, dihedral, and non-bonded pair interactions, respectively. The friction and stochastic driving force implicitly represents the effect of a solvent with a specified friction and temperature. The Langevin dynamics is integrated using a Velocity Verlet algorithm with a time step $\Delta t = 0.001 \tau_L$ and $\Gamma = 2 \tau_L$ using a customized version of LAMMPS [23,33].

Here and in the rest of the paper we use reduced units defined by the Langevin dynamics and DNA model. The unit of energy is $\epsilon = k_B T$, where we set Boltzmann's constant k_B to unity. The bead-to-bead distance along a single strand defines the unit of length σ which corresponds to the rise distance of DNA. The mass is $m = 1$ for all beads. A Langevin unit of time is defined as $\tau_L = \sigma \sqrt{m/\epsilon}$. The diffusion coefficient of DNA model strand is $D(n) = k_B T \Gamma / (m n)$ where n is the total number of beads. This can be equated with the DNA diffusion coefficient of a particular experimental conditions to obtain a time mapping. Extrapolating the data in Ref. [34] yields $\tau_L \approx 1.6 \times 10^{-12} s$ for $n = 20$.

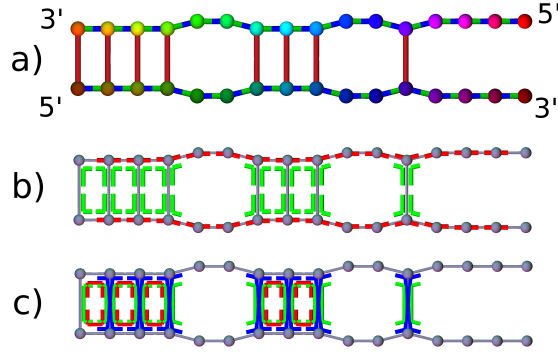


Figure 1. Illustrative DNA conformation. a) complementary beads, backbone and hybridization bonds, b) angular interactions indicated by two lines parallel to the involved bonds, c) dihedral interactions indicated by three lines parallel to the involved bonds. The figure is explained in the text.

Fig. 1a shows complementary nucleotide beads with the same hue but different levels of color saturation. As a simplification, we allow each bead only to hybridize with a single complementary bead. The DNA model has two types of bond interactions: permanent backbone bonds (shown green/blue) and dynamic

hybridization bonds (shown red). Backbone bonds and hybridization bonds are characterized by the two potentials:

$$U_{\text{bond,bb}}(r) = \frac{U_{\text{min,bb}}}{(r_c^{\text{b}} - r_0^{\text{b}})^2} ((r - r_0^{\text{b}})^2 - (r_c^{\text{b}} - r_0^{\text{b}})^2),$$

and

$$U_{\text{bond,hyb}}(r) = \begin{cases} \frac{U_{\text{min,hyb}}}{(r_c^{\text{h}} - r_0^{\text{h}})^2} ((r - r_0^{\text{h}})^2 - (r_c^{\text{h}} - r_0^{\text{h}})^2) & \text{for } r < r_c^{\text{h}} \\ 0 & \text{for } r \geq r_c^{\text{h}}. \end{cases}$$

In the simulations, we use $U_{\text{min,bb}} = 100\epsilon$, $r_0^{\text{b}} \equiv 1\sigma$, and $r_c^{\text{b}} = 1.2\sigma$, $r_0^{\text{h}} = 2\sigma$ and $r_c^{\text{h}} = 2.2\sigma$. Note that $U_{\text{bond,hyb}}(r) \leq 0$ for all distances. When two non-hybridized beads of complementary type are within a reaction distance r_c^{h} a hybridization bond is introduced between them. If they move further apart than r_c^{h} again, the hybridization bond is broken. The pair-interaction between beads is given by a soft repulsive potential, while we use the same potential for angular and dihedral interactions. They are given by

$$U_{\text{pair}}(r) = A \left[1 + \cos\left(\frac{\pi r}{r_c^{\text{p}}}\right) \right] \quad \text{for } r < r_c^{\text{p}},$$

where we use $A = 1\epsilon$ and $r_c^{\text{p}} = 1\sigma$ in the simulations, and

$$U(\Theta; \Theta_0, U_{\text{min}}) = -\frac{U_{\text{min}}}{2} (\cos[\Theta - \Theta_0] + 1),$$

Along the backbone of single strands we use a permanent angular interaction defined by $U(\Theta; \Theta_0 = \pi, U_{\text{min}} = 25\epsilon)$. This determines the persistence length of single strands. In Fig. 1b backbone angular interactions are shown as thick red lines around the central bead defining the angle.

In real DNA molecules, the hydrogen bonds between Watson-Crick complementary nucleotides act together with stacking interactions and the phosphodiester backbone bonds to give rise to a helical equilibrium structure of the double strand. In our coarse-grained model, we utilize angular and dihedral interactions to determine the ladder-like equilibrium structure of our DNA model. To control the stiffness of the double strands and to ensure anti-parallel 3'-5' alignment of the two single strands, we have assigned directionality to the backbone bonds [33]. This is also necessitated by the fact that the 3' and 5' carbons of the nucleotide sugar ring have been merged into the single nucleotide bead. Fig. 1a shows the backbone bonds colored green/blue to indicate the 3' and 5' ends, respectively.

When a hybridization bond is introduced, we also dynamically add angular interactions between the hybridization bond and the neighboring backbone bonds. These angular interactions are characterized by the potential $U(\Theta; \Theta_0 = \pi/2, U_{\text{min,a}})$, which favors a right angle conformation. When a hybridization bond is broken, concomitantly all the associated angular interactions are removed. In Fig. 1b the angular interactions are shown as green lines indicating the angle.

Besides introducing angular interactions, we also dynamically introduce dihedral interactions. A dihedral interaction involves four beads connected by three bonds, which defines a particular bond pattern, where the bonds can either be a hybridization bond, a $3' - 5'$ backbone bond, or a $5' - 3'$ backbone bond. Three bond patterns are possible. The bond pattern corresponding to red dihedrals in Fig. 1c, is characterized by $U(\Theta; \Theta_0 = 0, U_{\min, d})$ which favors a planar (cis) conformation. The bond pattern corresponding to blue dihedrals is characterized by $U(\Theta; \Theta_0 = \pi, U_{\min, d}, a = 0)$ which favors parallel backbone (trans) conformation. The last dihedral pattern corresponding to green dihedrals is characterized by $U(\Theta; \Theta_0 = 0, U_{\min, d})$ which favors a parallel (cis) conformation. Note that without the directional backbone bonds, we would not be able to distinguish between these two latter dihedral patterns.

During a simulation, at each time we introduce a hybridization bond, we also introduce up to four angular interactions and up to eight dihedral interactions, less if the hybridization bond is at the end of a strand. Let Δ be the total decrease in binding energy when two beads hybridize inside a chain, and we assign one third of this energy to bond, angular, and dihedral interactions, respectively. This choice does not affect the static properties of the model, which are determined by the total energy associated with a conformation, however it does influence the dynamic properties. Hence $U_{\min, \text{hyb}} = \Delta/3$, $U_{\min, a} = \Delta/12$, and $U_{\min, d} = \Delta/18$. We define $\Delta = 10\epsilon$ as a reference energy. Since only the ratio Δ/T enters the partition function of the model, this effectively fixes the absolute melting temperature of the stands. With the present model, the time spend per particle per step is approximately $1 \times 10^{-5}s$ on a standard PC.

3 Results

Three dimensional DNA structures can be built by utilizing the self-assembly properties of complementary strands and by linking several stands into a e.g. end-linked constructs. In particular, we have designed four constructs each comprising three end-linked 16 bead long strands. By programming the complementarity of the strands, we have designed the constructs to self-assemble into a tetrahedron[10,9]. We have also programmed the complementarity of 12 DNA constructs each comprising 5 end-linked 8 bead long strands. These constructs have been designed to self-assemble into an icosahedron[3]. We estimate that the melting temperatures are $T_m(8) \approx 1.3\epsilon$, and $T_m(16) \approx 1.6\epsilon$ from a separate set of melting simulations (not shown).

Fig. 2 shows visualizations of the DNA constructs during the self-assembly process. Initially the constructs are randomly placed into the simulation box. Progressively, complementary strands hybridize with each other, and the constructs form fragments that ultimately yield the designed target structures. The time scale of the self-assembly dynamics is determined by the time it takes the constructs to diffuse, collide, and hybridize completely. Since we have the simulation trajectory, we can also characterize the detailed time dependence of the self-assembly dynamics. Fig. 3 shows the fraction of hybridized bonds as a func-

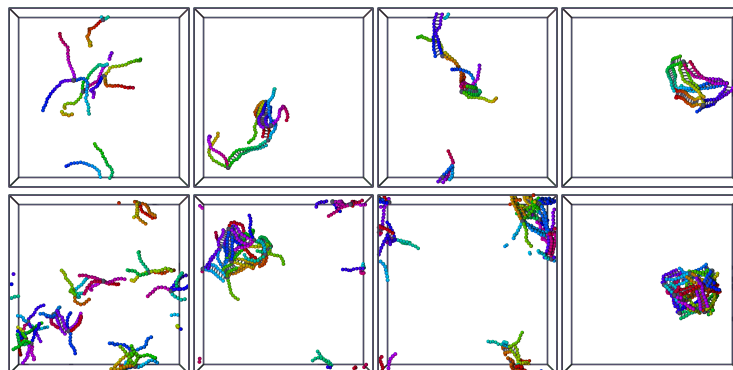


Figure 2. Self-assembly of a tetrahedron from four 3-functional DNA constructs (top row) and an icosahedron from twelve 5-functional DNA constructs (bottom row). Snapshots correspond to times $t = 1000\tau_L$, $10.000\tau_L$, $20.000\tau_L$, $50.000\tau_L$ steps (top row), and for $t = 1000\tau_L$, $20.000\tau_L$, $30.000\tau_L$, $60.000\tau_L$ steps (bottom row). Simulations have been performed at $T = 1.0\epsilon$. Note that periodic boundary conditions apply to the simulation box.

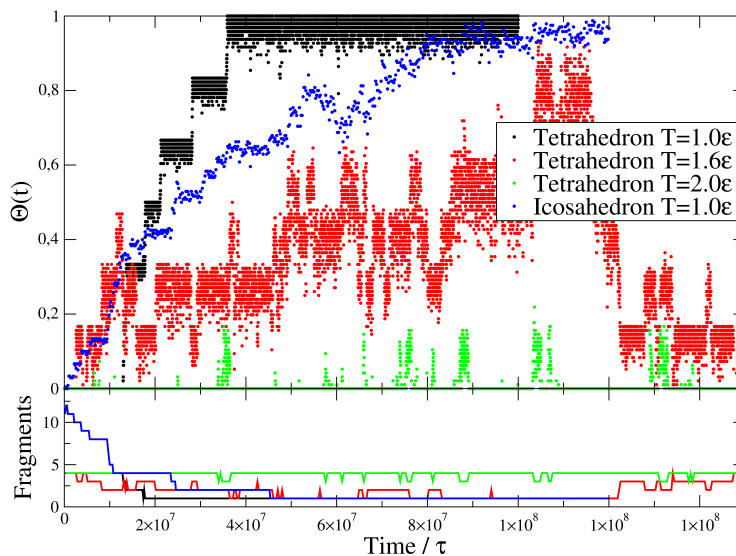


Figure 3. Fraction of hybridized bonds (top) and number of fragments (bottom) vs. time and temperature during the self-assembly of a tetrahedron and an icosahedron.

tion of time. By analyzing the bond structure, we can furthermore study the evolution of the number of structural fragments. For the icosahedron, we see a slow increase in the hybridized bond fraction towards unity as the structure is progressively assembled, while the number of fragments drops simultaneously from initially twelve free constructs to one when all constructs form a single icosahedron. However, even through we only have a single fragment, it takes further time for the remaining hybridization bonds to be formed. The equilibrium hybridization bond fraction does not appear to be reached at the end of the simulation at $1 \times 10^8 \tau$. For the tetrahedron, we observe a similar increase in the fraction of hybridized bonds, however with six distinct steps corresponding to the hybridization of each edge of the tetrahedron.

The self-assembly dynamics is stochastic and depends on initial conditions and random diffusive motion. We have run some of the simulations twice to see how they approach equilibrium along different trajectories. The equilibrium hybridization bond fraction appears to have been reached by the tetrahedron self-assembly simulations. For tetrahedra, we observe that self-assembly at higher temperatures leads to a marked decrease in the average hybridization bond fraction similar to melting of DNA double strands. At $T = 1.8\epsilon$ the temperature is above the melting temperature of the DNA constructs, and they only transiently hybridize. Since we have a single fragment at equilibrium, the bond reduction is most likely due to DNA bubbles. From the data sets we can estimate that the melting temperature of the tetrahedron i.e. $\Theta(T_m) = 0.5$ is approximately $T_m(\text{Tetrahedron}) \approx 1.5\epsilon$.

In the strand displacement approach to DNA computation, individual gates consist of one DNA template that is composed of several logical domains. In their initial state, all domains but one are hybridized to one or more complementary strands and are therefore inert. The only exposed single strand domain of each gate is a short toehold region at one end of the template. This toehold region can reversibly bind a complementary signal strand which is designed to be longer than the toehold domain and complementary to the next domain(s) of the template. The newly binding signal is then able to hybridize to all matching domains of the template, thereby displacing strands that were previously bound [37]. The displaced strands can be fluorescently marked output signals, or internal signals that can bind to toehold regions of downstream gates. By choosing domains of appropriate length, it can be guaranteed that toehold binding is reversible, whereas the final strand displacement is effectively irreversible, thus computation is energetically downhill and kinetically irreversible, if and only if the correct input strands are present and match the logical setup of the gates. It has been shown that this approach leads to modular logic gates that enable the design of large scale DNA circuits [5,15].

Fig. 4 shows simulations of the strand displacement process underlying Seelig et al.'s DNA computing approach [31]. The top row shows the successful displacement of an initially hybridized 12 bead long signal strand from a 20 bead long template by a 20 bead long signal strand: once the signal strand diffuses to and binds to the toehold region, branch migration occurs quickly (during 300 time

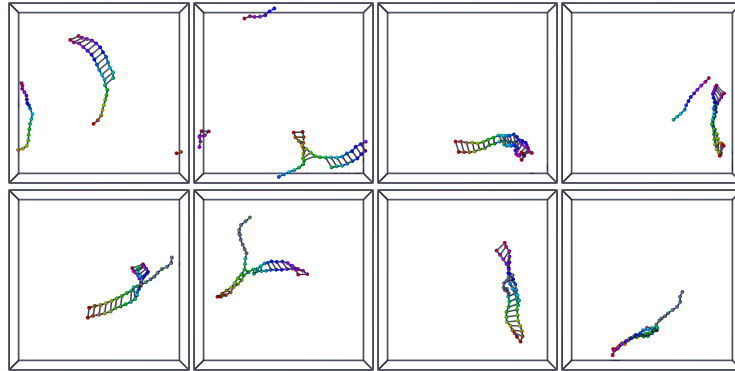


Figure 4. Simulations of strand displacement. A 20 bead long oligomer displaces a 12 bead long oligomer initially hybridized to a template for times $t = 500, 1.600, 1.700, 1.900\tau_L$ (top row). A 10 + 10 bead long oligomer where the latter half is non-complementary fails to displace a short oligomer hybridized to a template for times $t = 100, 3.000, 7.000, 10.000\tau_L$. Simulations are run at temperature $T = 1\epsilon$. Non-complementary beads are show as gray.

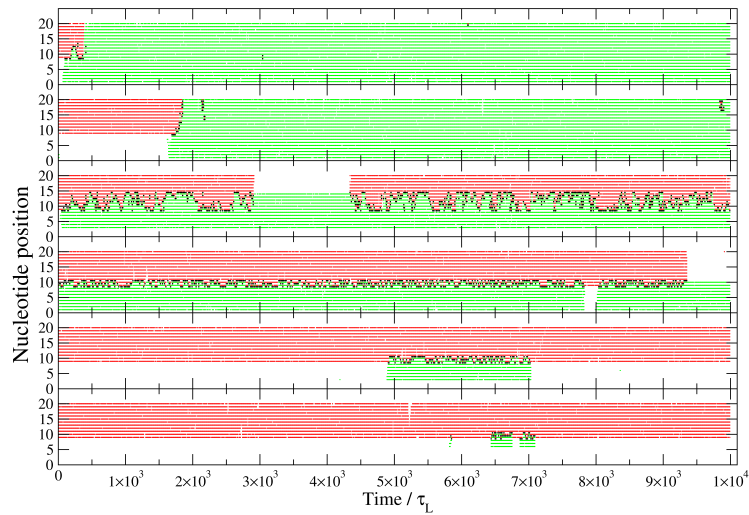


Figure 5. Time evolution of branch migration on individual template nucleotide beads. From top to bottom a) A 12 bead long oligomer (red) being displaced by a 20 bead long oligomer (green) on the template. b) a 20 bead long oligomer with different random conditions. c) 12 bead oligomer (red) competing with a 12 + 8 oligomer with 12 complementary and 8 non-complementary beads (green), d) a 12 bead oligomer (red) competing with a 10 + 10 oligomer, e) a 12 bead oligomer (red) competing with a 8 + 10 oligomer, f) a 12 bead oligomer (red) competing with 5 + 10 oligomer. Also shown is the branch migration point (black).

units) and the formerly bound signal strand is displaced irreversibly. The bottom row, on the other hand, shows how the displacement stalls in the presence of mismatches: here, a mismatch in the domain (last 10 beads) permits further hybridization of the signal strand. The newly binding and the original signal strand compete for matching bases in a random walk process until the non-matching strand dehybridizes again and leaves the gate available for potential matching signals (not present in the simulation).

Fig. 5 shows statistics of the displacement processes for several runs: the graphs depict hybridized bases of the original (red) and the newly binding signal strand (green), as well as the branch migration point (black). In the case of matching signals (top two simulations), it can be seen that displacement occurs quickly and essentially irreversible once the original strand is fully displaced. In the third simulation the signal strand and hybridized strand has the same length, and the interface is seen to diffuse forwards and backwards. A single dehybridization event is also observed for the original strand. In the case of mismatching signals (bottom three simulations), the displacement cannot proceed further than nucleotide 10, and the interface randomly moves between positions 8 and 10, until – occasionally – the mismatching signal dehybridizes from the toehold region (lack of green markers). In this case, the number of beads complementary to the toehold region (here 10, 8, and 5 beads) determines the equilibrium between hybridized and dehybridized configurations, and thus the performance and availability of the gate. Fig. 5 also depicts a source of potential failure in logical gates based on strand displacement, as the output signal can spontaneously dehybridize even in the absence of a matching input signal (as observed in the fourth simulation).

4 Conclusions

With these initial simulations, we have demonstrated that our coarse-grained DNA model can successfully simulate DNA assembly as well as DNA strand displacement dynamics which form the basis of state-of-the-art DNA computing approaches. We have successfully simulated self-assembly of DNA tetrahedra and icosahedra from four and twelve branched DNA constructs, respectively. Simulations show that the constructs self-assemble into the expected target structures.

We have further simulated successful displacement of an output strand when a matching input strand is present. In the presence of mismatches, we could demonstrate how the displacement process is prevented. Our simulations also capture potential failures of gates based on strand displacement, namely spontaneous release of the output strand in the absence of an input signal. These proof of concept simulations demonstrate how our coarse-grained model can be used to optimize the length and arrangement of toehold and domain structures in DNA computing approaches.

While such gate optimizations do not necessarily require spatially resolved models, our coarse-grained DNA model enables us to study systems that integrate DNA assembly and computing within a single framework. This enables us

to use these simulations as a starting point for building and testing statistical mechanical theories describing these complex systems.

5 Acknowledgements

The research leading to these results has received funding from the European Community's Seventh Framework Programme (FP7/2007-2013) under grant agreement no 249032 (MATCHIT). Funding for this work is provided in part by the Danish National Research Foundation through the Center for Fundamental Living Technology (FLinT).

References

1. Adleman, L.M.: Molecular computation of solutions to combinatorial problem. *Science* 266, 1021 (1994)
2. Andersen, E.S., Dong, M., Nielsen, M.M., Jahn, K., Subramani, R., Mamdouh, W., Golas, M.M., Sander, B., H., S., Oliveira, C.L.P., Pedersen, J.S., Birkedal, V., Besenbacher, F., Gothelf, K.V., Kjems, J.: Self-assembly of a nanoscale DNA box with a controllable lid. *Nature* 459, 73 (2008)
3. Bhatia, D., Mehtab, S., Krishnan, R., Indi, S.S., Basu, A., Krishnan, Y.: Icosahedral DNA nanocapsules by modular assembly. *Angew. Chem.* 121, 4198 (2009)
4. Brooks, B.R., Brooks, III, C.L., Mackerell, Jr., A.D., Nilsson, L., Petrella, R.J., Roux, B., Won, Y., Archontis, G., Bartels, C., Boresch, S., Cafisch, A., Caves, L., Cui, Q., Dinner, A.R., Feig, M., Fischer, S., Gao, J., Hodoscek, M., Im, W., Kuczera, K., Lazaridis, T., Ma, J., Ovchinnikov, V., Paci, E., Pastor, R.W., Post, C.B., Pu, J.Z., Schaefer, M., Tidor, B., Venable, R.M., Woodcock, H.L., Wu, X., Yang, W., York, D.M., Karplus, M.: CHARMM: The Biomolecular Simulation Program. *J. Comput. Phys.* 30, 1545 (2009)
5. Cardelli, L.: Strand algebras for DNA computing. *Nat. Comput.* 10, 407 (2011)
6. Case, D.A., Darden, T.A., Cheatham III, T.E., Simmerling, C.L., Wang, J., Duke, R.E., Luo, R., Walker, R.C., Zhang, W., Merz, K.M., et al.: AMBER 11. University of California, San Francisco (2010)
7. Cheatham III, T.E., Young, M.A.: Molecular dynamics simulation of nucleic acids: Successes, limitations, and promise. *Biopolymers* 56, 232 (2000)
8. Chen, J., Seeman, N.C.: Synthesis from DNA of a molecule with the connectivity of a cube. *Nature* 350, 631 (1991)
9. Erben, C.M., Goodman, R.P., Turberfield, A.J.: A self-assembled DNA bipyramid. *J. Am. Chem. Soc.* 129, 6992 (2007)
10. Goodman, R.P., Schaap, I.A.T., Tardin, C.F., Erben, C.M., Berry, R.M., Schmidt, C.F., Turberfield, A.J.: Rapid chiral assembly of rigid DNA building blocks for molecular nanofabrication. *Science* 310, 1661 (2005)
11. Hsu, C.W., Sciortino, F., Starr, F.W.: Theoretical description of a DNA-linked nanoparticle self-assembly. *Phys. Rev. Lett.* 105, 55502 (2010)
12. Jost, D., Everaers, R.: A unified description of poly- and oligonucleotide DNA melting: nearest-neighbor, Poland-Sheraga and lattice models. *Phys. Rev. E* 75, 041918 (2007)
13. Jost, D., Everaers, R.: A unified Poland-Scheraga model of oligo- and polynucleotide DNA melting: Salt effects and predictive power. *Biophys. J.* 96, 1056 (2009)

14. Jost, D., Everaers, R.: Prediction of RNA multi-loop and pseudoknot conformations from a lattice-based, coarse-grain tertiary structure model. *J. Chem. Phys.* 132, 095101 (2010)
15. Lakin, M.R., Youssef, S., Cardelli, L., Phillips, A.: Abstractions for DNA circuit design. *J R Soc Interface* 9, 470 (2012)
16. Langowski, J.: Polymer chain models of DNA and chromatin. *Eur. Phys. J. E Soft Matter* 19, 241 (2006)
17. MacKerell Jr, A.D., Banavali, N., Foloppe, N.: Development and current status of the CHARMM force field for nucleic acids. *Biopolymers* 56, 257 (2000)
18. Martinez-Veracoechea, F.J., Mladek, B.M., Tkachenko, A.V., Frenkel, D.: Design rule for colloidal crystals of DNA-functionalized particles. *Phys. Rev. Lett.* 107, 045902 (2011)
19. Ouldridge, T.E., Louis, A.A., Doye, J.P.K.: DNA nanotweezers studied with a coarse-grained model of DNA. *Phys. Rev. Lett.* 104, 178101 (2010)
20. Ouldridge, T.E., Louis, A.A., Doye, J.P.K.: Structural, mechanical, and thermodynamic properties of a coarse-grained DNA model. *J. Chem. Phys.* 134, 085101 (2011)
21. de Pablo, J.J.: Polymer simulations: From DNA to composites. *Annu. Rev. Phys. Chem.* 62 (2011)
22. Peyrard, M., Cuesta-Lopez, S., James, G.: Modelling DNA at the mesoscale: a challenge for nonlinear science? *Nonlinearity* 21, T91 (2008)
23. Plimpton, S.: Fast parallel algorithms for short-range molecular dynamics. *J. Comp. Phys.* 117, 1 (1995), <http://lammps.sandia.gov>
24. Poland, D., Scheraga, H.A.: Phase transitions in one dimension and the helix-coil transition in polyamino acids. *J. Chem. Phys.* 45, 1456 (1966)
25. Qian, L., Winfree, E.: Scaling up digital circuit computation with DNA strand displacement cascades. *Science* 332, 1196 (2011)
26. Rothemund, P.W.K.: Folding DNA to create nanoscale shapes and patterns. *Nature* 440, 297 (2006)
27. Sambriski, E.J., Ortiz, V., de Pablo, J.J.: Sequence effects in the melting and renaturation of short DNA oligonucleotides: structure and mechanistic pathways. *J. Phys. Condens. Matter.* 21, 034105 (2009)
28. Sambriski, E.J., Schwartz, D.C., de Pablo, J.J.: A mesoscale model of DNA and its renaturation. *Biophys. J.* 96, 1675 (2009)
29. SantaLucia, J.J., Hicks, D.: The thermodynamics of DNA structural motifs. *Annu. Rev. Biophys. Biomol. Struct.* 33, 415 (2004)
30. Savelyev, A., Papoian, G.A.: Chemically accurate coarse graining of double-stranded DNA. *PNAS* 107, 20340 (2010)
31. Seelig, G., Soloveichik, D., Zhang, D.Y., Winfree, E.: Enzyme-free nucleic acid logic circuits. *Science* 314, 1585 (2006)
32. Seeman, N.C.: Nucleic acid junctions and lattices. *J. Theor. Biol.* 99, 237 (1982)
33. Svaneborg, C.: LAMMPS framework for dynamic bonding an application modeling DNA. *Comp. Phys. Comm.* 183, 1793 (2012)
34. Tinlan, B., Pluen, A., Sturm, J., Weill, G.: Persistence length of single-stranded DNA. *Macromolecules* 30, 5763 (1997)
35. Winfree, E., Liu, F., Wenzler, L.A., Seeman, N.C.: Design and self-assembly of two-dimensional DNA crystals. *Nature* 394, 529 (1998)
36. Xhang, Y., Seeman, N.C.: Construction of a DNA-truncated octahedron. *J. Am. Chem. Soc.* 116, 1661 (1994)
37. Zhang, D.Y., Winfree, E.: Control of DNA strand displacement kinetics using toehold exchange. *J. Am. Chem. Soc.* 131, 17303 (2009)